2018 DIE CASTING CONGRESS & EXPOSITION
NADCA NORTH AMERICAN DIE CASTING ASSOCIATION

An Initial Evaluation of CT Scanning for Measuring and Characterizing Porosity in Aluminum Die Castings

Itamar Brill, Branden Kappes and Stephen Midson
Colorado School of Mines, Golden CO

ABSTRACT

Despite the fact that residual porosity is such a central aspect of the high pressure die casting process, there is little quantitative data available regarding porosity in aluminum die castings. CT scanning (computed tomography scanning) is a relatively new analytical technique that can provide detailed information on the number, size, distribution, and characteristics of porosity within components, and so has the potential to significantly increase knowledge with respect to porosity within die castings. CT scanning involves taking a large number of two-dimensional radiographic images as a casting is rotated in front of an x-ray beam, and utilizes digital geometry processing to generate a three-dimensional view showing the position and relative size of each and every pore within a casting.

This paper will report on an initial investigation to use x-ray micro-tomography on die castings to characterize the number, size and distribution of the porosity. For each of the castings, data reported includes a measurement of the average porosity content, the total number of individual pores, the distribution of the porosity across the width of the samples, and the thickness of the dense surface skin at different positions within the castings. Visual distributions of the porosity within each casting are also provided. An initial attempt was made to use sphericity values calculated from measured pore volumes and surface areas to distinguish between gas and shrinkage porosity.

INTRODUCTION

High pressure die casting involves the high speed injection of liquid metal into a hardened steel cavity, with high pressure applied to feed solidification shrinkage once the cavity has been filled. Die casting is used extensively for the production of aluminum components for a wide range of industries, as it is usually the lowest cost manufacturing process for the production of complex, 3-D shaped aluminum components. However, one of the most common drawbacks in the application of die castings is residual porosity[1], but despite its pervasiveness there is relatively little quantitative data available regarding the level and distribution of porosity in die castings. Even for something as straightforward as the total porosity content in a die casting, only limited quantitative data exits, partially due to the problems associated with quantitatively measuring porosity levels. Common techniques used to evaluate porosity in die castings include x-rays, metallographic sectioning and density measurements. For example, in an early paper, Linsey and Wallace[2] utilized density measurements to estimate that total porosity contents in aluminum die castings ranged between 0.5% and 4.1%, dependent upon processing conditions. However, density measurements provide no information on the size and distribution of the porosity, and little information on its source (entrapped air, lubricants, or shrinkage). Metallographic sectioning can provide additional details such as the location, size and origin of porosity, but obviously only for the specific location examined. X-ray testing is widely used within the die casting industry, but attaining quantitative information on porosity content from x-rays is notoriously difficult.

In addition, the porosity in die castings is normally not uniformly distributed within the components, but typically is located towards the center of the castings, with a dense skin forming at the surface (Figure 1)[3]. The dense surface skin is extremely important with respect to the performance of die castings, as it is crucial for pressure-tight applications, and has a significant

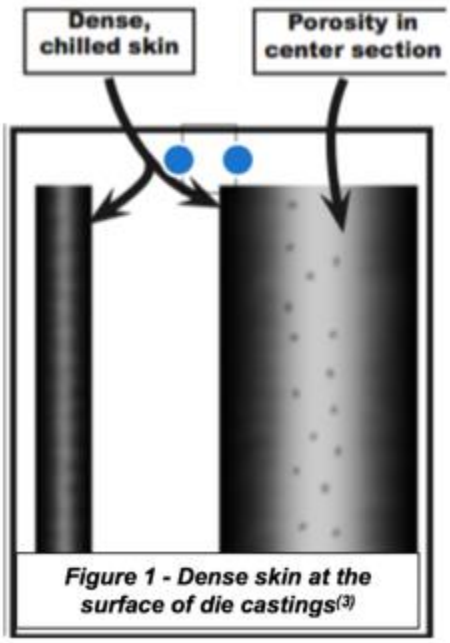

Figure 1 - Dense skin at the surface of die castings[3]

impact on mechanical performance. However, even less quantitative information is available regarding the thickness of the dense chilled skin, with published work suggesting the surface skin in die castings is around 0.5 mm [3-5]. The current authors are aware of no studies that identify parameters that affect the thickness of the dense skin.

X-ray computed tomography (CT) has the potential for providing a significant amount of quantitative data regarding the size, shape and distribution of pores within die castings and so has the potential to dramatically increase our knowledge with respect to porosity within die castings. CT scanning[6-8] is a nondestructive three-dimensional imaging technique in which volume reconstructions are produced from two-dimensional radiographs (projections) captured as the sample rotates relative to the direction of x-ray flux. Contrast in absorption radiographs is based on discrete differences in the x-ray attenuation throughout the sample volume. x-ray CT is an established method for evaluating defects in many types of materials[9-12], including characterization of porosity in cast aluminum[13-16]. There are a number of CT scanning processes available, including x-ray tomography, x-ray micro-tomography and neutron tomography, each having different levels of spatial resolution.

CT scanning is starting to be used as a quality control technique for die castings produced by commercial companies, but industrial applications typically utilize conventional x-ray tomography for the detection of large defects within castings (of the order of hundreds of micrometers). However, the focus of the current study was the detection of much smaller defects, to better characterize the size and distribution of all of the pores within the castings. This is similar to the approach used by Hairy et al.[13], but Hairy et al.[13] did not perform an extensive characterization of the size and distribution of the pores in their castings. It is the long term goal of the current researchers to utilize CT scanning to quantify the impact of die casting processing parameters on the size, volume and distribution of porosity within the castings, with the ultimate goal of identifying the processing conditions that minimize residual porosity contents, and maximize the thickness of the dense skin. In addition, it is known that the fatigue life of aluminum castings is controlled by the size of the largest pore[17], and data from Reference 17 reproduced in Figure 2 shows that fatigue life can be reduced by pores as small as 50-100 μm. Therefore, the current study is interested in the detection of pores approximately 50 μm and larger.

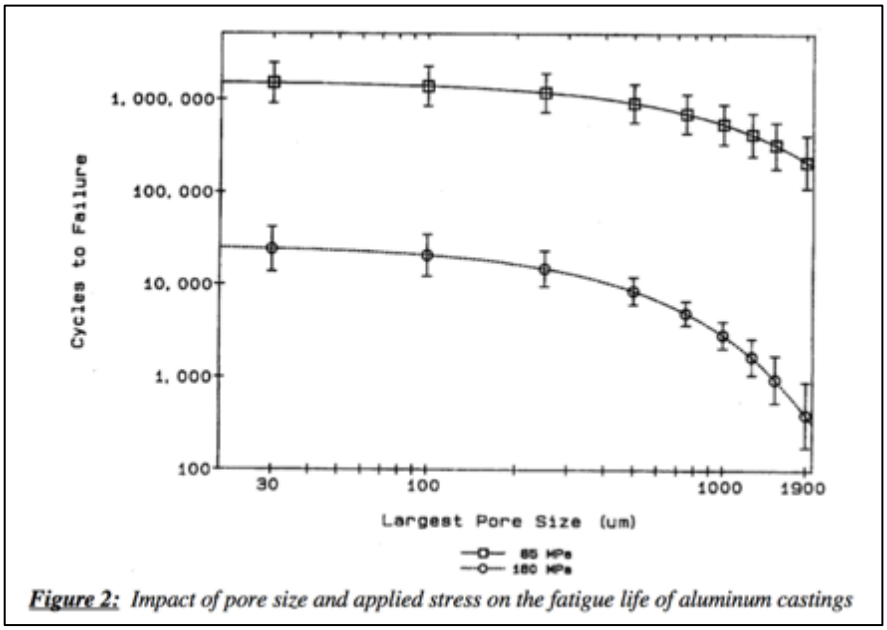

Figure 2: Impact of pore size and applied stress on the fatigue life of aluminum castings

Figure 2 – Impact of pore size and applied stress on the fatigue life of aluminum castings[17]

There are only a limited number of CT processes that are capable of detecting pores of this size in castings, while still providing the capability to examine castings of a size of commercial interest (multiple inches in size). Therefore, the objective of research currently being performed at the Colorado School of Mines (CSM) is to evaluate the capabilities of different CT scanning

processes, to determine which process exhibits the best capability for the characterization of die castings. For the current study, to detect pores as small as 50 μm, an x-ray micro-tomography unit was used. This unit, and the process parameters used to measure and characterize the porosity, are described in more detail in the following section.

EXPERIMENTAL PROCEDURES

Die cast-to-size tensile bars were used for this study. The bars were cast from alloy 383 produced using the two dies shown in Figure 3. The shape of the tensile bars are shown in Figure 4[18], and research by one of the authors has demonstrated that these as-cast tensile bars can achieve handbook data properties for aluminum die castings[19].

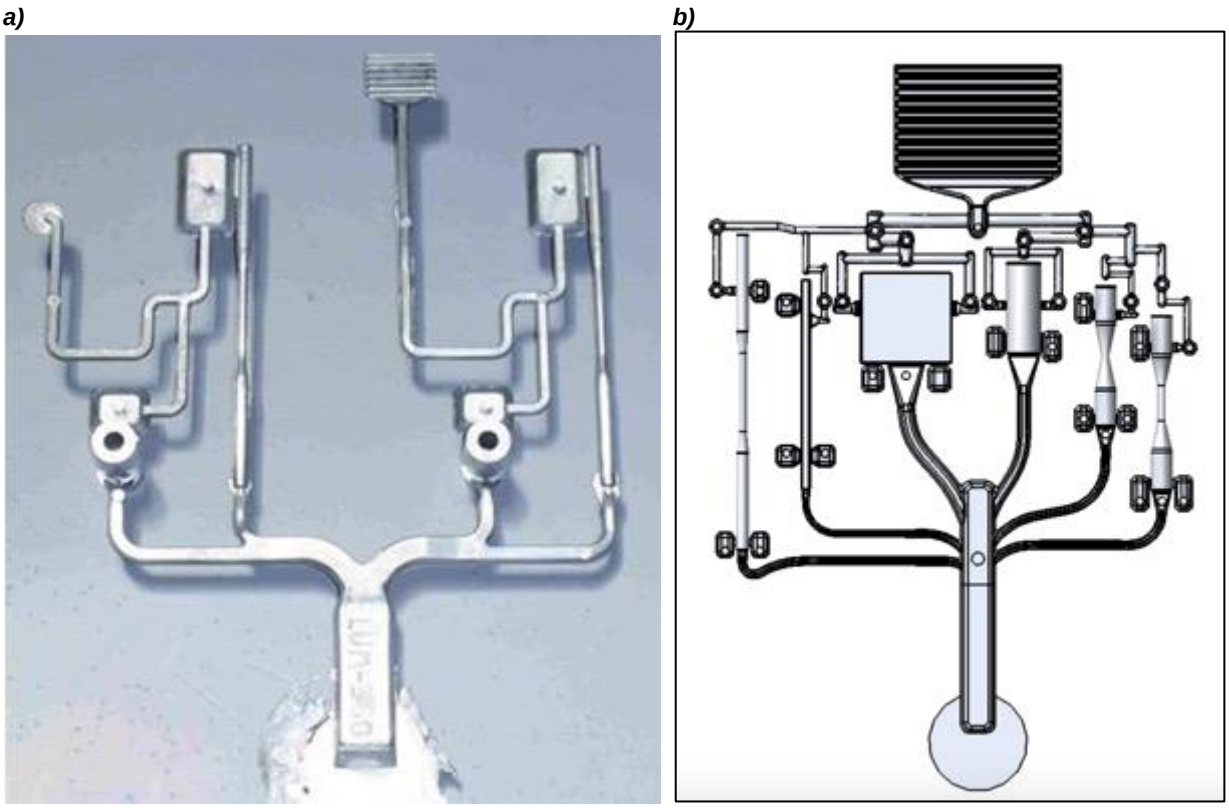

Figure 3 – Two mechanical property test dies used to produce the tensile bars
(a) Premier die
(b) NADCA die

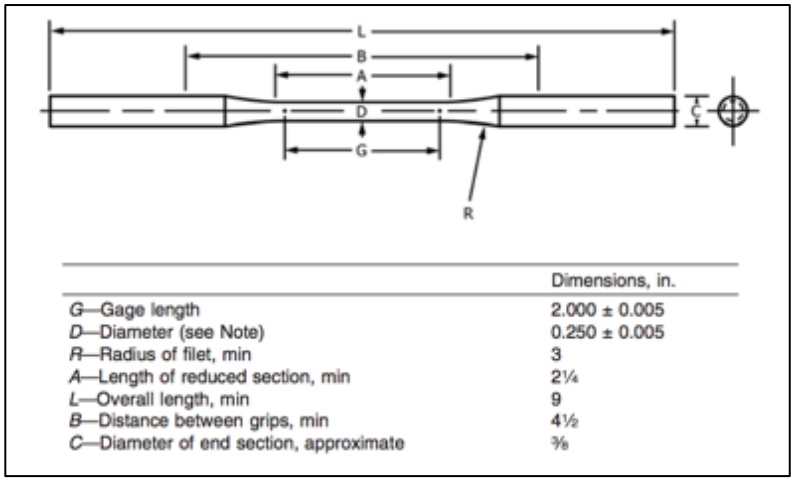

	Dimensions, in.
G—Gage length	2.000 ± 0.005
D—Diameter (see Note)	0.250 ± 0.005
R—Radius of filet, min	3
A—Length of reduced section, min	2¼
L—Overall length, min	9
B—Distance between grips, min	4½
C—Diameter of end section, approximate	⅜

Figure 4 – Standard cast-to-size tensile bar for die castings[18]

Small sections were cut from two of the tensile bars (one produced using the Premier die and one produced using the NADCA die.) As shown in Figure 5, both of the tensile bar castings were gated at one end of the bar, but as shown in Figure 6, the gates for the two castings were different, with the gate for the Premier tensile bar being close to the full diameter of the tensile bar grip, while the gate for the tensile bar produced in the NADCA die was essentially a semi-circle.

The location of the samples evaluated by CT scanning (shown in Figure 5) was purposely chosen to include both gage and grip sections from the tensile bar, with the grip section being taken from the side of the casting away from the gate. As shrinkage porosity in the castings was fed from the biscuit, along the runner and through the gate, and the smaller diameter gage will solidify before the larger diameter grip, so there should be a larger amount of shrinkage porosity in the grip as compared with the gage section.

Figure 5 – Photograph of tensile bar, showing the location of the scanned sample

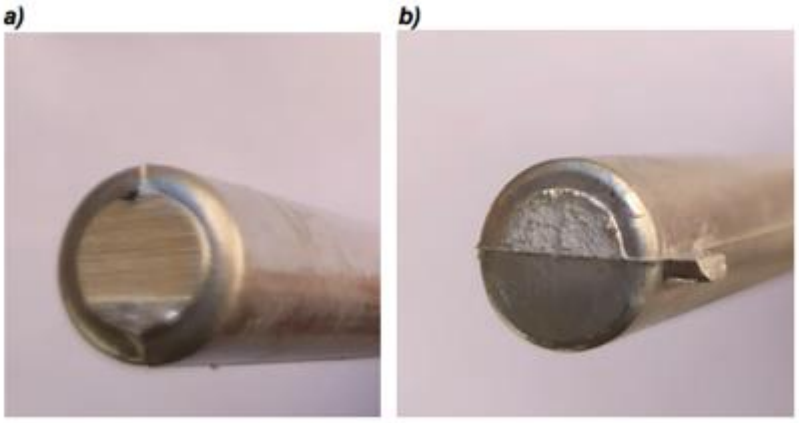

Figure 6 – Gates used on the two tensile bars
a) Full circular gate used on the Premier tensile bar
b) Semi-circular gate used on the NADCA tensile bar

X-ray micro-tomography measurements were conducted on a ZEISS Xradia 520 Versa microscope (Carl Zeiss X-ray Microscopy Inc., Pleasanton, CA). An annotated picture of the data collection chamber is shown in Figure 7. An electron current, accelerated through an adjustable potential, incident on a tungsten anode produces a divergent, broad-spectrum X-ray beam (i.e., white beam) with energies in the range of 30–160 keV. Die cast aluminum samples were imaged at 80 kV with and a beam current of 11.4 mA onto a 1024×1024 detector with 24 µm pixels The source position (α=25 mm), detector position (β=145 mm), and optical magnification (0.4X) results in a total magnification of:

$$M = m_{\text{optical}} \cdot m_{\text{geometric}} = 0.4\frac{\alpha+\beta}{\alpha} = 0.4 \cdot 5.8 = 2.32$$

Using this factor, the 242 µm^2 pixel on the detector projects back to a 10.12 µm^2 area in the sample. A 10.1 µm resolution allows for identification of pores with an effective diameter of 30.3 µm and quantitative shape determination (< 3% error in distance) of pores with an effective diameter greater than 101 µm[20].

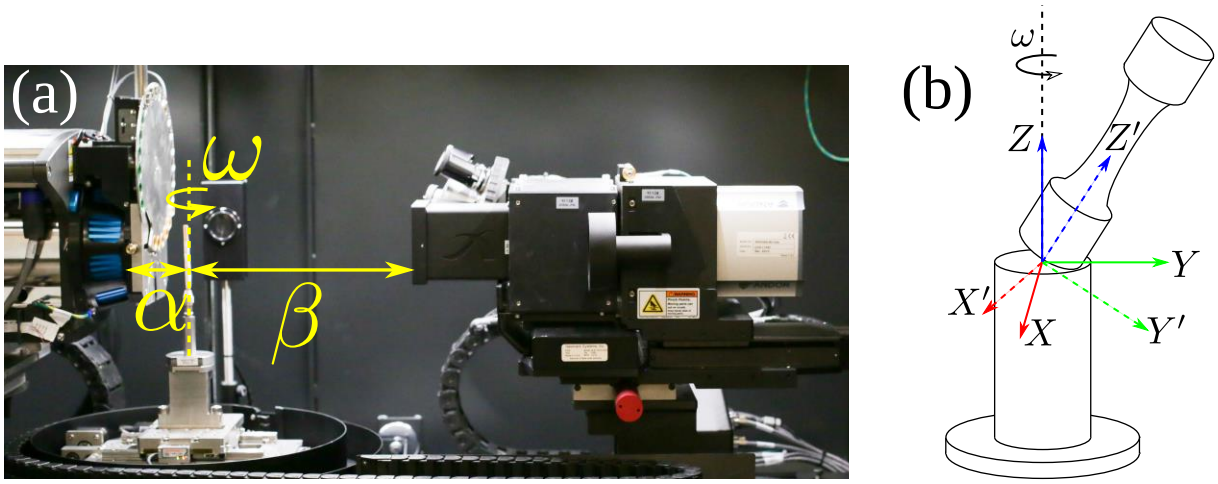

Figure 7 - (a) Image of the X-ray computed tomography (CT) data collection chamber. The source, left, is α mm from the sample rotation axis; a scintillation detector is β mm to the right. Under X-ray illumination, the scintillation detector fluoresces in proportion to the incident flux, producing a grayscale image that is collected by a 16-bit CCD camera (far right). (b) Schematic of the sample stage, sample, and lab coordinate system (solid lines), and one sample coordinate system (dashed lines). The actual sample tilt has been exaggerated to emphasize the distinction between these two coordinate systems.

Segmentation of porosity from metal matrix produces two distinct Regions of Interest (ROIs). A marching cubes algorithm[21] is then used to differentiate connected components in the ROI of the air. Of these connected components, those volumes that intersect any corner, edge or surface of the reconstructed volume are external to the part, all other volumes in the air ROI are internal voids. The volumes, surface areas, centers of mass, and shapes of these voids are calculated and tabulated.

Unlike the volumes and areas of the pores, the centers of mass and orientations of the pores are dependent on the reference coordinate system. Therefore, these latter features must be transformed from the laboratory coordinate system (i.e., parallel and perpendicular to the x-ray beam) to a sample coordinate system (i.e., parallel and perpendicular to the sample's axis), such as that shown in Figure 7b. The precise orientation of the sample is more accurately measured from the collected data. The X-ray CT produces a regular grid of intensities, which can be considered an intensity field mapped to a 3D point cloud. The centers of mass of each N voxels (N on the order of 1-7 billion) in the sample are collected as below and decomposed using a singular value decomposition.

$$X = \begin{pmatrix} x_1 & y_1 & z_1 \\ \vdots & \vdots & \vdots \\ x_N & y_N & z_N \end{pmatrix} = U\Sigma V^T$$

U, V^T, and Σ are the left and right singular vectors and the singular vectors, respectively. The right singular vectors, V^T, are the eigenvectors of $X^T X$. These vectors have two important properties. They are orthonormal, which means they are mutually perpendicular unit vectors that span a 3D space. Secondly, they are oriented such that the first right singular vector minimizes the variance of the projections along this collection of N coordinates, i.e. the first singular vector points along the long axis of the sample. The second and third singular vectors are radial. Finally, the product $U\Sigma$ are the coordinates of the voxels in the new sample-centric coordinate system. For a sufficiently uniform pore distribution, as observed in these samples, the SVD can equally be applied to the pore positions to identify the sample coordinate system to make calculation of the SVD more computationally tractable.

For each scan, a large amount of data was collected, including the volume, surface area, position and dimensions of each pore. This allowed the calculation of the aspect ratio, as well as the sphericity of each pore. Sphericity (Ψ) was calculated using the following equation:

$$\Psi = \frac{\pi^{1/3}(6V_p)^{2/3}}{A_p}$$

where V_p and A_p are the volume and surface area of each pore, respectively. Another useful parameter that is more meaningful to the average caster than the volume of a given pore is its equivalent diameter[13], which is the diameter of a pore of a given volume assuming it is a perfect sphere. The equivalent diameter (D) can be calculated from the volume as follows:

$$D = 2\left(\sqrt[3]{\frac{3V_p}{4\pi}}\right)$$

RESULTS AND DISCUSSION

TENSILE SAMPLE PRODUCED IN NADCA DIE

Figure 8 shows scans indicating the location of the porosity in the NADCA tensile bar sample. The sample contained 64,685 pores larger than 36 μm in size. The total volume of porosity was 28,368,517,344 μm^3 (28.4 mm^3), and as the sample weight was 6.09 grams, the average porosity content was 1.3%. However, as shown in Figure 8, the porosity is clearly not uniformly distributed, with more pores in the grip area, and a wide dense skin. In addition, analysis of the raw data collect from the CT scan indicated that the average porosity content in the gage section was 0.3%, while it was 1.7% in the larger diameter grip section (regions where these measurements were performed are defined in Figure 9). As noted previously, it is not surprising that the porosity content was higher in the grip region, as the gage region will solidify before the grip, blocking feeding from the biscuit. In addition, the expansion in cross-section as the liquid metal flows from the gage to the grip will likely cause additional entrapment of air in the grip. Both of these are probably the reason for the higher level of porosity in the grip.

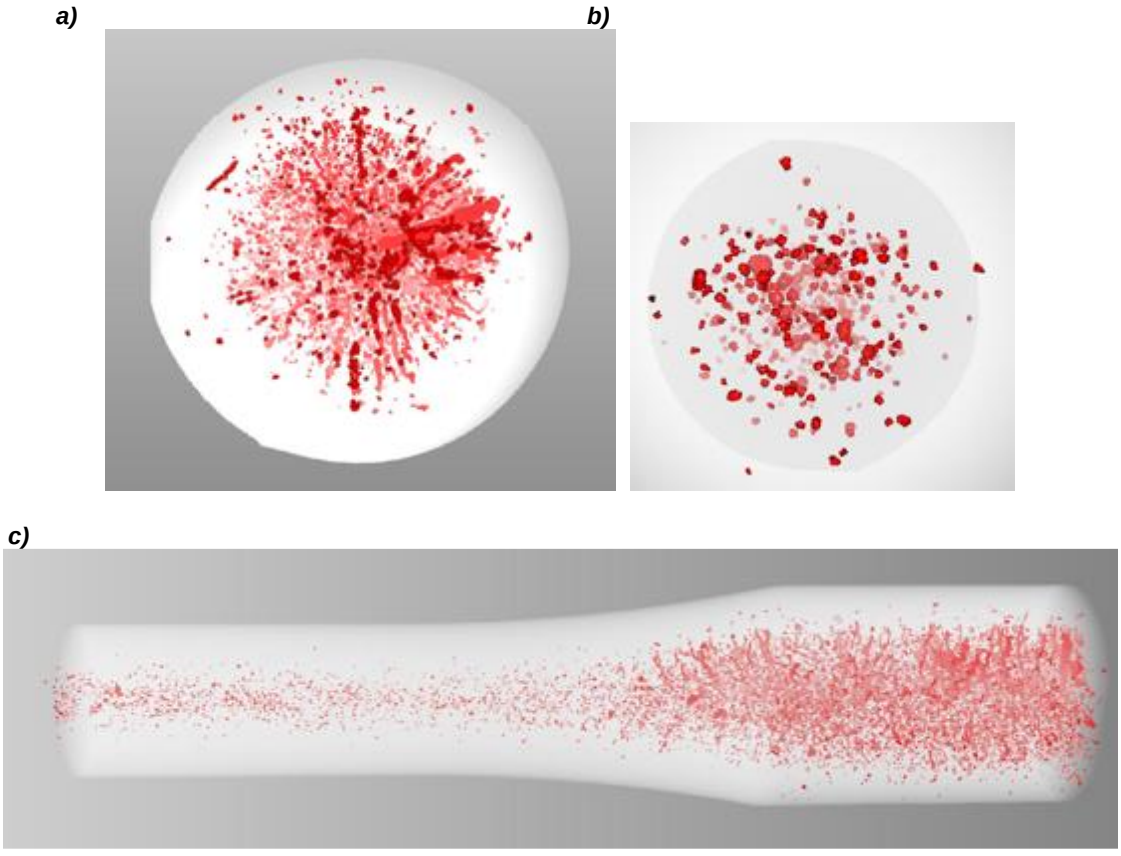

Figure 8 – Showing the porosity distribution in the NADCA tensile bar sample
(a) Grip section
(b) Gage section
(c) Longitudinal view

TENSILE SAMPLE PRODUCED IN PREMIER DIE

Figure 9 shows the distribution of porosity in the tensile sample produced in the Premier die. This sample contained 86,696 pores larger in size than 37 μm. The total volume of the porosity was 16,600,925,090 μm^3 (16.6 mm^3), and as the sample weighed 6.6 grams, the average porosity content within the entire sample was 0.7%. The fact that the Premier sample contained more individual pores as compared with the NADCA sample, while having a lower total porosity content suggests that the median pore size was smaller for the Premier samples, and this was confirmed by an examination of the raw data. The median pore volume for the NADCA sample was 87,342 μm^3 (equivalent diameter of 55 μm) while the volume of the pore was 31% smaller (60,384 μm^3, equivalent diameter of 49 μm) for the tensile sample produced in the Premier die.

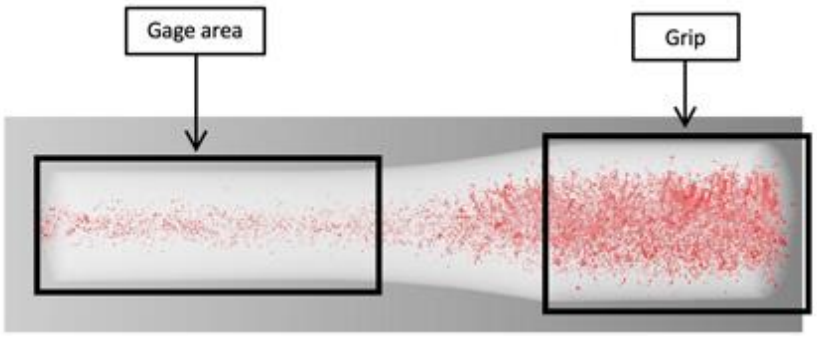

Figure 9 – Regions of gage area and grip section analyzed

Again the porosity is not uniformly distributed (either radially or along its length) in the Premier tensile bar. An analysis of the raw data indicated that the average porosity content in the gage section was 0.4%, while in the grip section it was 1.1%.

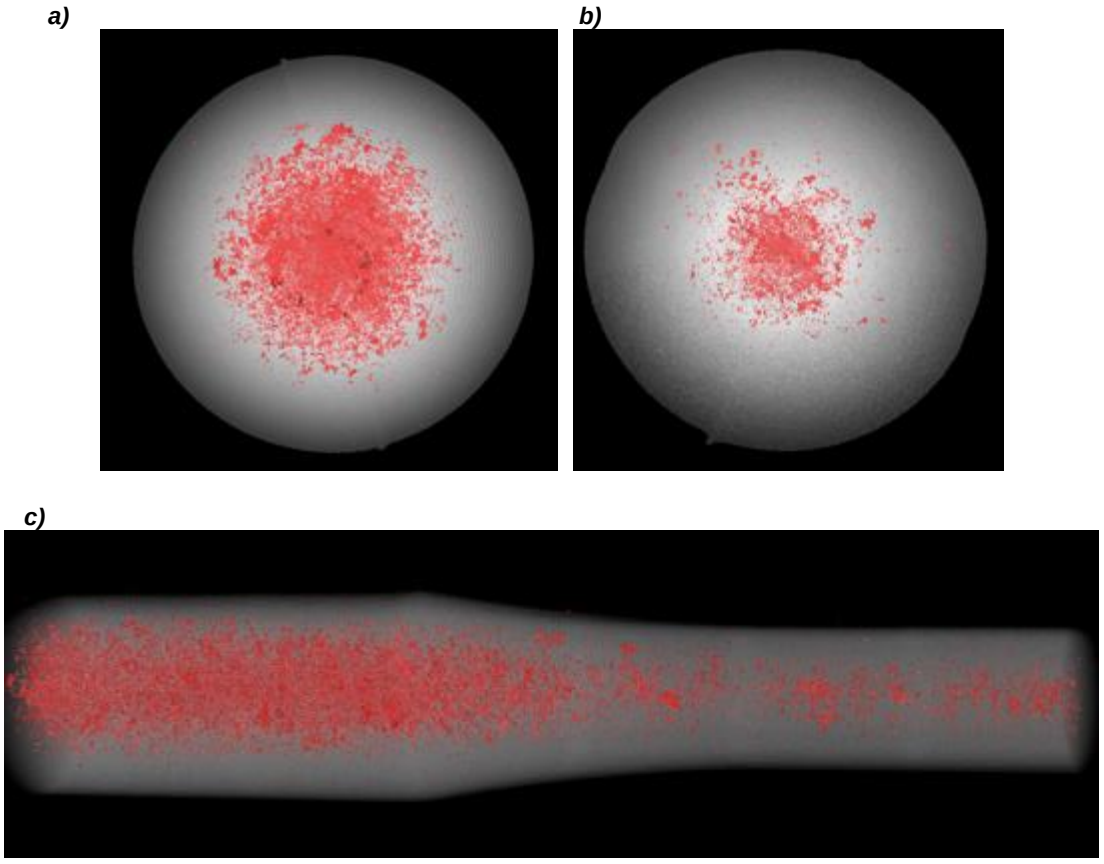

Figure 10 – Showing the porosity distribution in the Premier tensile bar sample
(a) Grip end
(b) Gage length
(c) Longitudinal view

RADIAL DISTRIBUTION OF POROSITY

Clearly the porosity in the two samples is not uniformly distributed, with much of the porosity being located close to the centerline of the samples, with a relatively wide porosity-free dense skin. Based on the porosity distribution shown in Figures 8c and 10c, an estimate can be made of the thickness of the dense skin. This is obviously relatively imprecise in nature, but was estimated from the longitudinal views for each of the samples. These values are listed in Table 1.

Table 1 – Estimates of the thickness of the dense skin based on the scans shown in Figure 6c and 8c

Sample	Thickness of the Dense Skin (mm)	
	Gage Section	Grip Section
NADCA tensile bar	1.7	1.0 to 1.1
Premier tensile bar	1.0 to 1.3	1.4 to 1.9

The raw data collected from the two CT scans can also be used to quantitatively characterize the porosity distribution in a radial direction (i.e., from centerline to surface). This was performed by dividing up the 3/8-inch (~9.5 mm) diameter grip region of the tensile bars into ten concentric rings, each 0.5 mm width (as shown schematically in Figure 11a). The smaller diameter gage section of the bars (1/4-inches, or 6.4 mm) was divided up into seven concentric rings, each 0.5 mm width (as shown schematically in Figure 11b). Using the raw data collected from scans, the porosity content of each of the rings was calculated and is plotted in Figures 12 and 13.

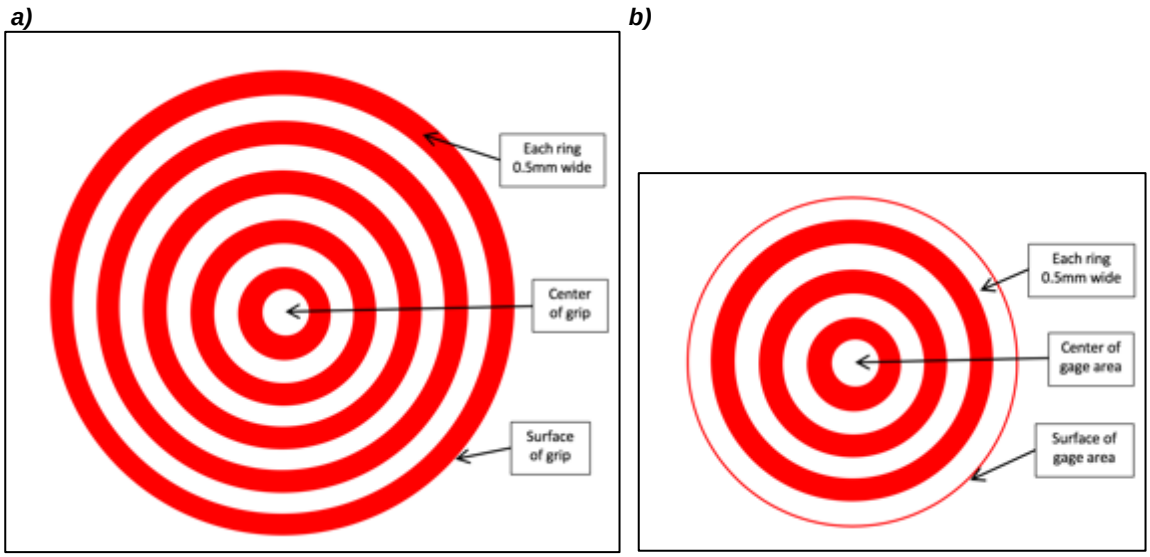

Figure 11 – Schematic representation showing how the grip region was divided into 10 concentric rings (each 0.5 mm wide), and the gage section was divided into seven concentric regions

The data presented in Figures 12 and 13 show that the porosity content at the centerline of both the grip and gage sections of the tensile bar are around 4-5%, but quickly drop off towards their surfaces.

The thickness of the dense surface skin can also be estimated from the porosity profiles shown in Figures 12 and 13. The approach used in this study was to assume that the dense skin starts when the porosity level reaches 0.1%. Based on this relatively arbitrary approach, the estimates of skin thickness are listed in Table 2. Interestingly, there appears to be little correspondence between the skin thickness estimates produced from the visual scans (data in Table 1) and from the porosity distribution measurements (data in Table 2). One reason may be the relatively coarse ring thickness used to calculate the porosity profiles shown in Figures 12 and 13 – using a narrower ring thickness may produce more accurate porosity profiles, and help to estimate the dense skin thickness more accurately.

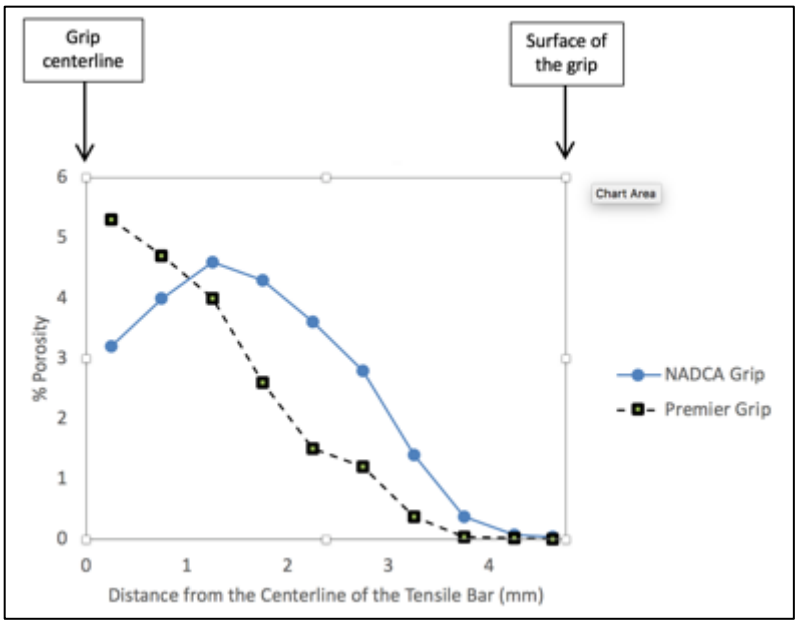

Figure 12 - Distribution of porosity from the centerline to the surface area of the grip portion of the two tensile bars

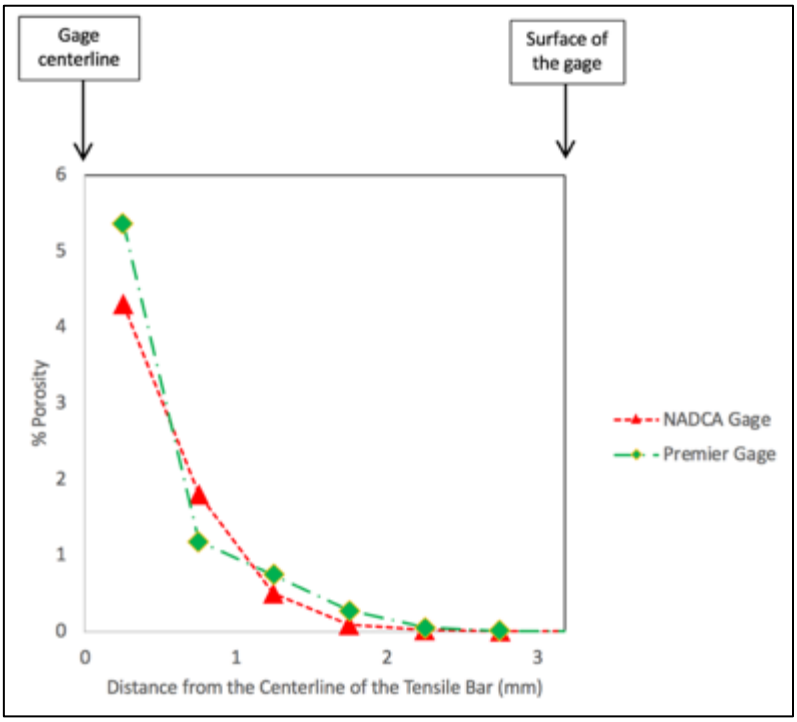

Figure 13 - Distribution of porosity from the centerline to the surface area of the gage portion of the two tensile bars

Table 2 – Estimates of the thickness of the dense skin based on the porosity profiles shown in Figures 11 and 12

Sample	Thickness of the Dense Skin (mm)	
	Gage	Grip
NADCA	0.6	1.5
Premier	1.1	1.1

DISTINGUISHING BETWEEN SHRINKAGE AND GAS POROSITY

An initial attempt has been made to utilize the calculated sphericity to distinguish between the gas porosity and shrinkage porosity in the tensile bars. As is well known, gas porosity in castings is relatively spherical in nature, and so should have a relatively high value of sphericity (close to unity). Shrinkage porosity, however, is typically more irregular shaped, as it has to conform to the surface contours of the surrounding dendrites, and so its sphericity value should be much lower than unity. Using the same approach as shown in Figure 11, the grip and gage sections of the two tensile bars were divided into concentric rings each 0.5 mm wide, and the average (mean) sphericity in each ring calculated. These are plotted in Figure 14, along with the porosity measurements shown in Figures 12 and 13. Interestingly, for three of the samples, the values of average sphericity increase significantly close to the surface of the samples, where only gas porosity might be expected to exist. This suggest that sphericity may be a parameter that can be used to distinguish between gas and shrinkage porosity in the CT scans, and will be examined in more detail in future studies.

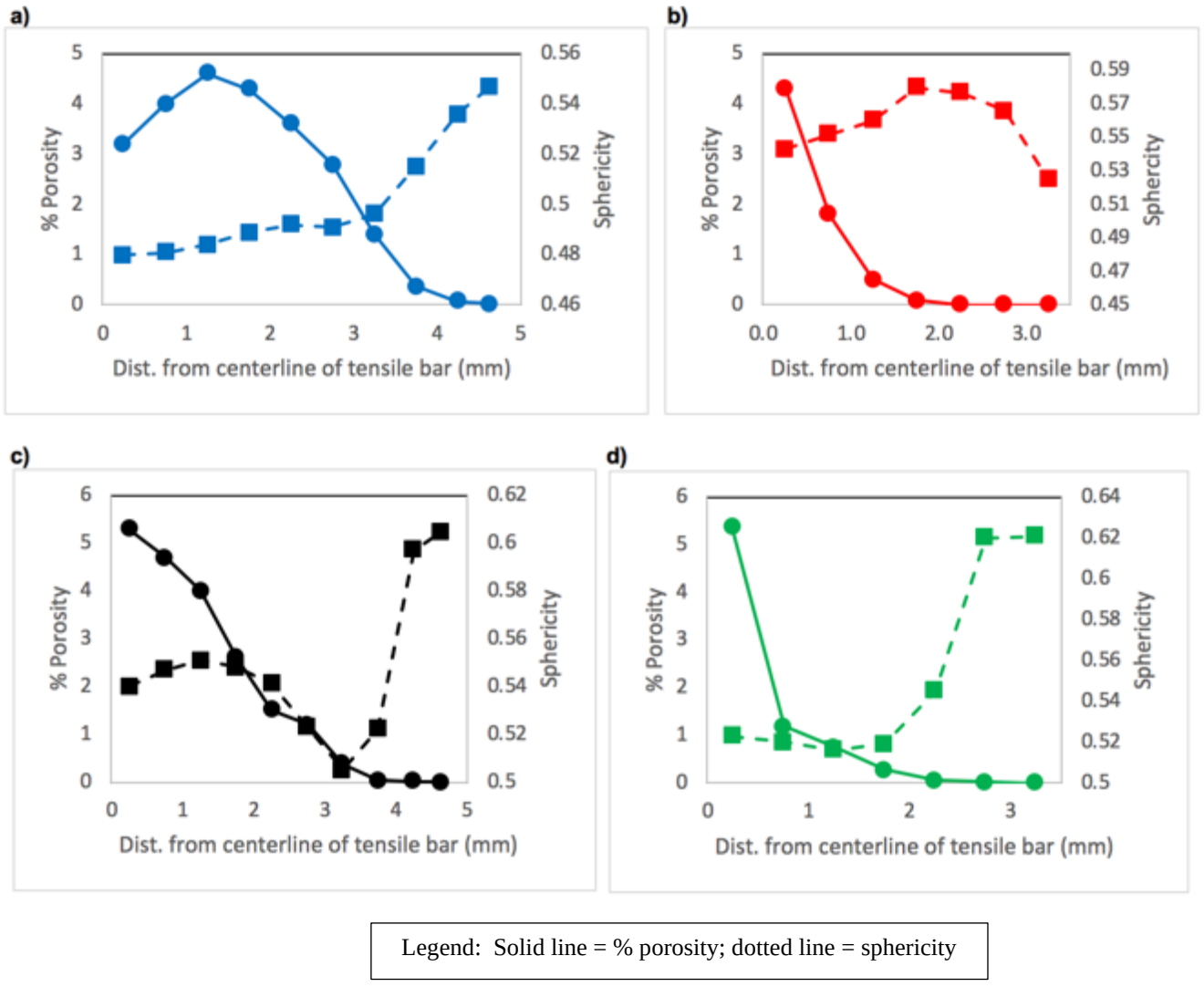

Legend: Solid line = % porosity; dotted line = sphericity

Figure 14: Relationship between percent porosity and sphericity
a) NADCA grip
b) NADCA gage
c) Premier Grip
d) Premier gage

SUMMARY & CONCLUSIONS

1. The objective of this study was to use x-ray micro-tomography (CT scanning) to examine the size and distribution of porosity in high pressure die castings. The samples chosen for this preliminary study were sections approximately two-inches long cut from cast-to-size tensile bars produced in two different dies (the Premier die and the NADCA die). The micro-tomography process was capable of identifying pores larger than about 36 μm in size.
2. Scans are presented showing the location and distribution of the porosity. The sample produced in the NADCA die contained more than 64,000 pores larger than 36 μm in size, and it had an average porosity content of 1.3%. However, the pores were not uniformly distributed in the sample, with more pores in the grip section of the sample (than in the gage section), and both the grip and gage had a relatively thick dense surface section.
3. The sample produced in the Premier die contained a larger number of pores (more than 86,000 pores greater than 37 μm in size), but a lower average porosity content of 0.7%. Again the pores were not uniformly distributed.
4. Analysis of the pore distribution in a radial direction showed that both samples had a porosity content of around 4-5% at their centerlines, and very low porosity concentrations (<<1%) close to their surfaces. Two approaches were used to attempt to characterize the thickness of the dense skin, but gave significantly different values.
5. An initial attempt was made to utilize calculated sphericity values (calculated using the measured volume and surface area of each pore) to distinguish between gas and shrinkage porosity. As gas porosity is normally more spherical in nature, it should have a higher value of sphericity, while shrinkage pores should have lower sphericity values. An initial analysis was promising, as it indicated that pores close to the surface have higher values of sphericity, and it is likely that most of these are gas pores. However, significantly more analysis will need to be performed to determine whether these x-ray micro-tomography measurements are actually capable of distinguishing between gas and shrinkage porosity.

ACKNOWLEDGMENT

The authors would like to acknowledge the North American Die Casting Association (NADCA), who provided the funding for this research.

REFERENCES

1. V. D. Tsoukalas, St. A. Mavrommatis, N. G. Orfanoudakis and A. K. Baldoukas, A study of porosity formation in pressure die casting using the Taguchi approach, Proc. Instn. Mech. Engrs. Vol. 218 Part B: J. Engineering Manufacture Paper B10103
2. D. Lindsey & J.F. Wallace, Effect of Vent Size and Design, Lubrication Practice, Metal Degassing, Die Texturing and Filling of Shot Sleeve on Die Casting Soundness, Proceedings 7th SDCE International Die Casting Congress, 1972, 1-15
3. Product Design for Die Casting, 6th Edition, Published by the North American Die Casting Association, 2015
4. Andrew Borland and Naoyuki Tsumagari, "The Significance of The Die Cast Skin Pertaining to the Fatigue Properties of ADC12 Aluminum Alloy Die Castings", 110th Metal Casting Congress, 2006, paper no. T06-031
5. P. Weiler, J.T. Wood, R.J. Klassen, R. Berkmortel, G. Wang, Variability of skin thickness in an AM60B magnesium alloy die-casting, Materials Science and Engineering A 419, 2006, 297–305
6. S. R. Stock, "X-ray microtomography of materials", Int. Mater. Rev. 44, 1999, 141-464
7. L. Salvo, P. Cloetens, E. Maire, S. Zabler, J. J. Blandin, J. Y. Buffière, W. Ludwig, E. Boller, D. Bellet, C. Josserond, "X-ray micro-tomography an attractive characterization technique in materials science", Nucl. Instrum. Methods B, 200, 2003, 273-286
8. E. N. Landis, D. T. Keane, "X-ray microtomography", Mater. Charact. 61, 2010, 1305-1316
9. F. Beckmann, R. Grupp, A. Haibel, M. Huppmann, M. Nöthe, A. Pyzalla, W. Reimers, A. Schreyer, R. Zettler, "In-Situ synchrotron X-ray microtomography studies of microstructure and damage evolution in engineering materials", Advanced engineering materials, 9, 2007, 939-950
10. E. Maire, P. J. Withers, "Quantitative X-ray tomography", International Materials Reviews, 59, 2014, 1-43
11. R. Cepuritis, E. J. Garboczi, S. Jacobsen, "Three dimensional shape analysis of concrete aggregates fines produced by VSI crushing" Powder Technology, 308, 2017, 410-421
12. J. F. Barrett, N. Keat, "Artifacts in CT: Recognition and avoidance" RadioGraphics, 24, 2004
13. Patrick Hairy, Yves Gaillard, Valeris Buecher & Amaury Chabod, Quantification of Defects in Pressure Die Casting (Part III), 3D Analysis by Tomography, Fonderie et Fondeur d'Aujourd'hui, No. 271, January, 2008, p. 8-22
14. Nicoletto, Gianni, Giancarlo Anzelotti, and Radomila Konečná. "X-Ray Computed Tomography vs. Metallography for Pore Sizing and Fatigue of Cast Al-Alloys." Procedia Engineering 2, no. 1, 2010, 547–54
15. Alejandro Golob, "Quality Control Best Practices: Introducing Industrial CT Scanning into Your Quality Assurance Process", Die Casting Engineer, May 2015, p 14

16. Andrew Good, “Industrial CT at a Glance”, Die Casting Engineer, September 2013, p 40
17. J.F. Major, Porosity Control and Fatigue Behavior in A356-T61 Aluminum Alloy, Trans. American Foundry Society, 1997, 901
18. ASTM B557-15, Standard Test Methods for Tension Testing Wrought and Cast Aluminum- and Magnesium-Alloy Products, Pub. ASTM, 2015
19. S.P. Midson, J.A. Brennan and J. Bell, “Impact of Heat Treatment Parameters and Magnesium Concentration on the Mechanical Properties of Alloy 380-type Conventional Die Castings after T5 Heat Treatment”, NADCA 2012 Congress, paper no. T12-021
20. Branden Kappes, Senthamilaruvi Moorthy, Dana Drake, Henry Geerlings, and Aaron Stebner. “Machine Learning to Optimize Additive Manufacturing Parameters for Laser Powder Bed Fusion of Inconel 718.” In *Proceedings of the 9th International Symposium on Superalloy 718 and Derivatives: Energy, Aerospace, and Industrial Applications*, 2018, 595–610
21. William E. Lorensen, and Harvey E. Cline. “Marching Cubes: A High Resolution 3D Surface Construction Algorithm.” *SIGGRAPH Comput. Graph.* 21, no. 4, August, 1987, 163–69